JOURNAL OF PROPULSION AND POWER
Vol. 11, No. 3, May–June 1995

Investigation of Scramjet Injection Strategies for High Mach Number Flows

D. W. Riggins*
University of Missouri–Rolla, Rolla, Missouri 65401-0249
C. R. McClinton† and R. C. Rogers‡
NASA Langley Research Center, Hampton, Virginia 23681
and
R. D. Bittner§
Analytical Services and Materials, Hampton, Virginia 23681

A method for estimating the axial distribution of thrust performance potential in a supersonic combustor is described. A complementary technique for illustrating the spatial evolution and distribution of thrust potential and loss mechanisms in reacting flows is developed. A wall jet case and swept ramp injector case for Mach 17 and Mach 13.5 flight enthalpy inflow conditions, respectively, are numerically modeled and analyzed using these techniques.

Introduction

THE development of a hypersonic vehicle utilizing air-breathing engines requires the injection and burning of hydrogen into a predominately supersonic airstream. The injection and subsequent combustion of the fuel in the combustor releases energy that is, at best, partially recovered in the nozzle and along the afterbody. This recovery is manifested by the development of vehicle thrust power. Due to strong shocks and viscous layers generated upstream of the combustor by the drag-producing forebody and inlet, the entering flow into the combustor can be highly nonuniform, with regions of both high- and low-thrust work availability. (Thrust work availability is defined as the potential for usefully generating vehicle thrust work by expanding the flow to pressure or a fixed area ratio.) In the combustor, downstream-directed injection of gaseous hydrogen takes place either from injector ramps or from flush-wall orifices. Both of these injection strategies rely on the generation of strong counter-rotating spillage-induced vortices in the flow for near-field entrainment and mixing of the fuel with the oxidizer.[1] Downstream of the injection region, fuel mixing (with subsequent combustion) takes place due to both vortex action and smaller scale turbulent diffusion. Thrust work availability is destroyed in the burner by injector blockage, mixing, wall heat transfer, and frictional drag on the injector surface and combustor walls. Generally, it is increased by injection momentum, possible base pressurization, and the release of energy into the flow by exothermic chemical reaction; however, dissociation reactions involving both oxygen and nitrogen can be significant in reducing actual energy availability. The flow at the exit of the combustor is then expanded in the nozzle and along the afterbody where the bulk of the useful work potential of the flow is realized by the generation of vehicle thrust. Additional losses in thrust work availability within the nozzle are due primarily to wall shear. Some recombination can occur as the flow expands and cools in the nozzle. This results in an additional increase in thrust work potential. In general, the flow through a practical scramjet engine is highly three dimensional with embedded regions of both increasing and decreasing thrust potential. The evolution and distribution of these regions are due to complex and interrelated physical mechanisms. The ultimate engineering significance of any engine analysis, experiment, or numerical simulation must be measured by its success in increasing understanding of the ability of the engine to efficiently produce thrust. In addition, such studies must lead to the accurate estimation of the thrust potential for use in vehicle design efforts.

Extensive experimental and numerical studies have been undertaken in the past seven years in order to study supersonic mixing and reacting flows. Much of the earlier computational fluid dynamics (CFD)-related effort was directed at the numerical simulation of simplified supersonic mixing and reacting shear layers.[2] More recently, application of CFD to complex three-dimensional reacting flows has been moderately successful in the prediction of certain basic performance quantities such as fuel distribution, bulk mixing, and combustion efficiency, as well as wall pressure and, less successfully, wall heat flux.[3] Unfortunately, most of these verification studies are for lower flight Mach numbers ($M < 8$) due to the limited data base at higher Mach numbers. This article presents some results of detailed numerical studies of two injector configurations at high-enthalpy flight conditions. The first configuration examined is a 30-deg downstream-angled flush wall jet in Mach 17 enthalpy flow for which experimental data is available. Because this configuration was not originally designed for the purpose of demonstrating performance, a swept-sided ramp in the identical combustor duct at a flow enthalpy corresponding to a flight Mach number of 13.5 is then modeled with flow conditions (temperature and pressure) and jet conditions more closely matched to actual flight conditions. The main goal of this article is to use these solutions to demonstrate the ability of CFD to quantify combustor thrust potential, to identify thrust gain and loss regions, and to visualize the spatial distribution and evolution of thrust potential in scramjet combustors.

Earlier work on flow losses has been performed by many workers, notably by Swithenbank[4] who identified concerns

Presented as Paper 92-3287 at the AIAA/SAE/ASME/ASEE Joint Propulsion Conference and Exhibit, Nashville, TN, July 6–8, 1992; received July 29, 1993; revision received Sept. 26, 1994; accepted for publication Nov. 16, 1994.

*Assistant Professor, Department of Mechanical and Aerospace Engineering. Member AIAA.
†Head, Numerical Applications Office. Member AIAA.
‡Senior Research Engineer, Hypersonic Propulsion Branch. Member AIAA.
§Research Engineer, Numerical Applications Office. Member AIAA.

with mixing enhancement strategies that could entail greater flow losses than performance gains recovered from the additional mixing. Czysz and Murthy[5] present an excellent treatment of work availability (or exergy) in high-speed propulsion systems; this follows work done by Builder[6] who applied energy availability analysis to the Brayton cycle engine. The work presented here follows previous work done by the authors.[7,8] Traditionally, total pressure loss has been used as a measure of flow loss in a system (as it is related directly to the irreversible entropy increase). It is difficult, however, to meaningfully quantify total conditions for very high Mach number flows due to issues related to isentropic compression of such a flow to Mach zero. The results of this work are organized into two parts: first, flowfield characteristics of mixing and reaction are discussed and presented for a flush-wall injector at Mach 17 flight enthalpy. An additional swept-ramp injector case is formulated that more closely simulates actual combustor conditions for a flight Mach number of 13.5. Secondly, the evolution and distribution of thrust potential for these configurations are investigated in detail in order to explain and visualize combustor performance.

Combustor Thrust Potential

The approach taken here in order to analyze and present thrust potential (or flow losses) is twofold. First, the three-dimensional CFD-generated flow can be suitably one dimensionalized. The one-dimensionalization scheme used here (specific details can be found in Ref. 8) identically conserves all mass fluxes (including individual species mass fluxes), momentum fluxes, and energy fluxes between the three-dimensional solution and the one-dimensional representation of the solution. Hence, using this method, mass, momentum, force, and energy distributions in an axial sense are exactly duplicated. It should be noted that there can be a significant difference between flow parameters such as pressure and temperature as obtained by using this method and as obtained when using conventional averaging techniques that do not in general satisfy conservation of all fluxes. This difference has been observed to be large for mixing and reacting nonuniform flow. The one-dimensionalization method used here has been made practical by the large quantity of flowfield information generated by CFD solutions. It is only as accurate (in the limited context of a one-dimensional representation) as the three-dimensional CFD solution from which it is generated.

The flux-equivalent one-dimensionalized flow obtained by using this method is then expanded (from a given plane) in an ideal or reference nozzle (generally allowing no further mixing of unburned fuel). The flow is taken either to a fixed area ratio or an ambient pressure in order to obtain a net thrust or, more properly, a net thrust potential. Specifically, the combustor inflow stream thrust is subtracted from the stream thrust of the flow at a given crossflow plane in the combustor that has been expanded isentropically to the reference condition. This yields the following analytical definition for the (net specific) thrust potential (i.e., available thrust over mass flow rate of airstream):

$$\frac{T}{\dot{m}_{\text{air}}} = \frac{\int_e (\rho u^2 + P)\, dA - \int_i (\rho u^2 + P)\, dA}{\int_i \rho u\, dA}$$

where e represents conditions at the exit of the reference expansion, i represents conditions at the combustor inflow, and ρ, u, and P are the fluid density, velocity, and pressure, respectively. Hence, with this particular definition of thrust potential, the combustor inflow has a net positive thrust potential associated with it. For this investigation, the reference condition chosen for the expansion process is chosen to be an arbitrary low pressure (P_e = 500 Pa). However, for actual design purposes, a fixed area ratio expansion process is recommended when using this technique.

The net thrust potential obtained can be nondimensionalized by defining a combustor effectiveness parameter.[8] The denominator of this parameter is the net thrust generated by isentropically slowing the combustor entrance flow to Mach zero, ideally adding heat, and expanding isentropically to the reference condition. However, for high-enthalpy flows such as examined in this work, the stagnation conditions are difficult to quantify. For this reason, as well as to provide actual performance (net specific) thrust potential is used in this work. The reference nozzle quasi-one-dimensional expansion can be done by specifying either complete reaction (i.e., all available mixed fuel and oxidizer produce water at stoichiometric proportions), equilibrium, or chemically frozen flow, or some combination of these methods. In this work, all reference expansions are done using complete reaction.

The result of applying this technique to a typical scramjet combustor CFD solution is shown schematically in Fig. 1, which illustrates the typical idealized axial distribution of thrust potential vs combustor axial distance for a swept-ramp-fueled combustor (as illustrated in Fig. 2). First, the inflow plane itself has some thrust-generating potential as discussed above; hence, the curve begins with finite thrust potential at the combustor entrance. Upstream of the injection region (A to B) there is frictional drag on both combustor walls and on injector ramp surfaces as well as shock waves due to ramp or jet compression of the flow and possible boundary-layer buildup along walls and corners. There can also be pressure drag on forward-facing injector surfaces. These loss mechanisms result in a decrease in thrust potential. The region of the flow be-

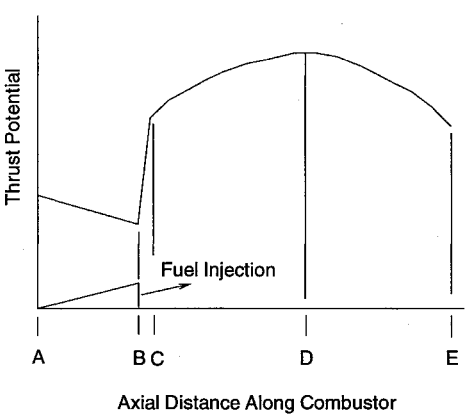

Fig. 1 Schematic of typical thrust potential distribution along combustor (injector ramp case).

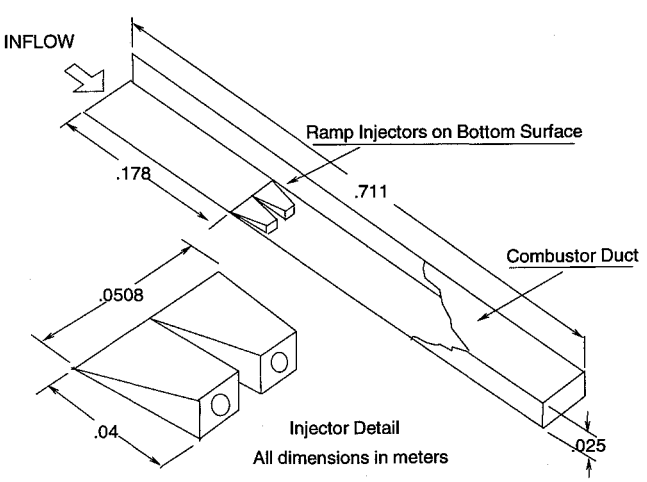

Fig. 2 Combustor duct with injector ramps (flush-wall jet orifices located at approximately the same axial location as ramps).

Table 1 Case description and conditions

Case no.	Description	Nominal duct inflow conditions				Nominal injection conditions (hydrogen)				Combustor wall temperature
		Gas	P, kPa	T, K	M	P, kPa	T, K	M	Φ	T_w, K
1	30-deg flush wall	Air	16.5	2089	5.75	671.0	244	1.0	3.0	300
2[a]	Swept ramp	Air	136.0	1342	5.0	2120.0	704	1.7	1.0	1366

[a]Computational case (no experimental data available).

tween B and C is dominated by the injection of fuel itself (i.e., from the base of a ramp); the sharp increase in thrust potential is due to the jet momentum addition to the flow and base pressure force on the injection ramps. Note that the jet contribution to the thrust potential can be a significant part of the overall combustor thrust potential.

Exothermic reaction occurs in region C to E and is responsible for increasing the thrust potential; in this region the benefit of energy release associated with the combustion overcomes flow losses. Finally, the flow region between D and E is dominated by the gradual loss of thrust potential due to the local effect of wall shear and reflecting shock structures. Heat release in this region slows due to the depletion of available fuel and oxidizer. Region A–C for flush-wall jet configurations may be somewhat obscured by the axial spread of momentum from the jet orifice. Also, a small amount of hydrogen entrainment and burning upstream of the wall jet (through the wall boundary layer) can actually cause a slight increase in thrust potential from A to B. Note that this method yields a straightforward estimate of the optimal combustor length. The actual optimal length may well be somewhat less than that indicated by point D on the sketch due to vehicle weight and component integration considerations.

The limitations of this method are associated with the one dimensionalization of a highly complex nonuniform flowfield and with uncertainties associated with the reference nozzle expansion process. For instance, the one dimensionalization of a three-dimensional flow results in an irreversible gain in entropy that is analogous to that occurring in a multistream mixing process. In addition, a large quantity of information is inevitably discarded in the one-dimensionalization process. It is physically possible that some fraction of the angular momentum in three-dimensional vortical structures at the combustor exit can transfer to streamwise momentum within the nozzle, or vice versa. Such structures, along with effects of strong shocks and expansions and additional mixing and finite rate chemistry effects in the nozzle itself, are, by necessity, lost in the thrust potential estimation method described above. Another important effect of the one dimensionalization in terms of reacting flows is the loss of information regarding the actual temperature, velocity, and fuel/oxygen spatial distributions and their strong coupled effect on details of the kinetics, heat release, and irreversible entropy gains. The relative importance of this effect will depend on the manner in which the reference expansion is done (i.e., frozen, finite rate, equilibrium, or complete reaction).

The second phase of this work has been to individually expand the flow in each cell (or streamtube) of a flowfield plane in a numerical solution. This is done in a manner similar to that discussed above for the one-dimensional method. This technique results directly in the ability to study in detail the spatial distribution of thrust potential for the combustor and also allows investigation of the effect of the one dimensionalization on the prediction of thrust potential. In this method, the resulting summation (over a crossflow plane) of the thrust potential of each individual cell yields nozzle exit stream thrusts that can be compared to the results of the one-dimensional method. The difference in net thrust potential predicted between the methods has been observed to be as large as 10% in the injection near field where the flow is highly nonuniform and issues associated with one dimensionalization are significant. However, the average difference in thrust potential as predicted by the two methods across all combustor crossflow planes for the cases examined in this work is less than 2%.

Experimental Configuration

The facility used to generate the high-enthalpy data (corresponding to a flight Mach number of 17) used in this study was the NASA HYPULSE facility located at GASL (General Applied Science Laboratory).[9] This is a high-enthalpy expansion tube (previously the Langley Expansion Tube) facility with about a 0.5-ms steady-state test duration. The combustor model had a rectangular cross section with a single flush-wall injector angled downstream at 30 deg centered in the duct or two side-by-side swept ramps (see Fig. 2) with hydrogen injection from the base. Cross-sectional duct dimensions were 2.54 cm (vertical) by 5.08 cm. The combustor was about 70 cm long with the injector located at the 18-cm station. Experimental instrumentation included pressure gauges that were located on the centerline of both lower and upper surfaces. Nominal inflow and jet exit conditions for the cases analyzed are presented in Table 1. The second case listed in this table is a computational study only of a swept ramp injector in this duct. This is a Mach 13.5 flight enthalpy case and was simulated with air inflow pressure and temperature and hydrogen fuel temperature close to the anticipated vehicle operating conditions. It provides a realistic (though subscale with excessive wetted perimeter) combustor geometry case with flight-scaled jet and inflow conditions.

Codes and Computational Approach

The NASA Langley Research Center Spark family of codes[10–12] is used in this work. This includes a time-dependent three-dimensional full Navier–Stokes solver and a marching [or parabolized Navier–Stokes (PNS)] version. There has been extensive validation of these codes for supersonic reacting flowfields.[13,14] For this work, a modified algebraic model has been used to generate the turbulent viscosity. This model is easy to use and has been successfully applied for mixing prediction in injector flows.[15] In addition, a turbulent Schmidt number of 0.5 is used for all cases in this study.[16,17] This approach represents a modeling technique for prediction of downstream bulk mixing and mean flow. Details of the highly complex turbulence field are not accurately predicted by this model. The reactions are simulated using a seven-reaction, seven-species finite rate model that is a subset of that used by Drummond.[10]

The computational approach taken in this work is summarized below. Upstream (from the test section entrance to a location three diameters upstream of the bow shock structure of the injector), the parabolized version of the Spark code is used in order to generate a fixed inflow for the near field (which is highly elliptic in character), of the jet region. For the ramp case, the elliptic calculation begins at the ramp leading edge. The outflow plane from the upstream PNS solution is used as the fixed inflow for the elliptic jet region where the time-dependent Navier–Stokes Spark code is applied. The exit plane of the elliptic domain is chosen suffi-

ciently far away from the injector to allow successful downstream marching computations. This corresponds to one ramp length downstream of the ramp base for the ramp case and five jet diameters downstream of the jet orifice for the flush-wall case. Solution convergence in the elliptic near field is defined by a matrix of criteria that includes unchanging time-averaged values of wall pressures and mixing efficiencies, mass flow conservation (both fuel and air), and relatively unchanging values of one-dimensionalized parameters describing the flow.[8] Overall mass flow at the near-field region exit is monitored to ensure a level of less than 1% conservation error. When these criteria are met, the elliptic region is considered to be converged and the outflow is then passed to the parabolized code for the downstream computation. This technique works well for both mixing and reacting high-speed combustor modeling and has successfully simulated numerous experimental flows. The ability to run the parabolized code in the downstream section vastly decreases computer requirements.

For all sections (inflow, near-field, and far-field), the cross-flow plane grid used is 51 × 31 for the wall jet and 61 × 61 for the swept ramp case. In the elliptic (near-field) zones, the wall jet case has 41 axial points while the ramp case has 81 axial points. The jet orifices are modeled as approximately rectangular in both cases. Grid clustering is used at all walls and symmetry planes and on all solid surfaces for the ramp solution. The 30-deg wall jet case, however, treats the side wall as an inviscid wall.

A related investigation[3] using the Spark codes demonstrated grid convergence for parameters such as fuel mixing and wall pressures when using similar spatial resolutions and geometries in the Hypulse duct. The wall temperature is held constant at 300 K for the wall jet case (Mach 17 enthalpy; pulse facility) and 1366 K for the swept ramp case (flight Mach number = 13.5). The flow is considered to be laminar upstream of the jet (or ramp), but is tripped to turbulent through the jet on the injection wall (or at the ramp leading edge for the ramp case). For the top wall, the flow is tripped at the approximate location of the bow shock impingement.

Results and Discussion

The first part of this section describes flowfield characteristics and mixing and combustion efficiencies for a 30-deg flush-wall jet with a fuel equivalence ratio of 3.0 in a simulated flight Mach 17 enthalpy flow. Additionally, in order to study a case with conditions more representative of actual flight operation, a swept ramp at flight Mach 13.5 enthalpy is nu-

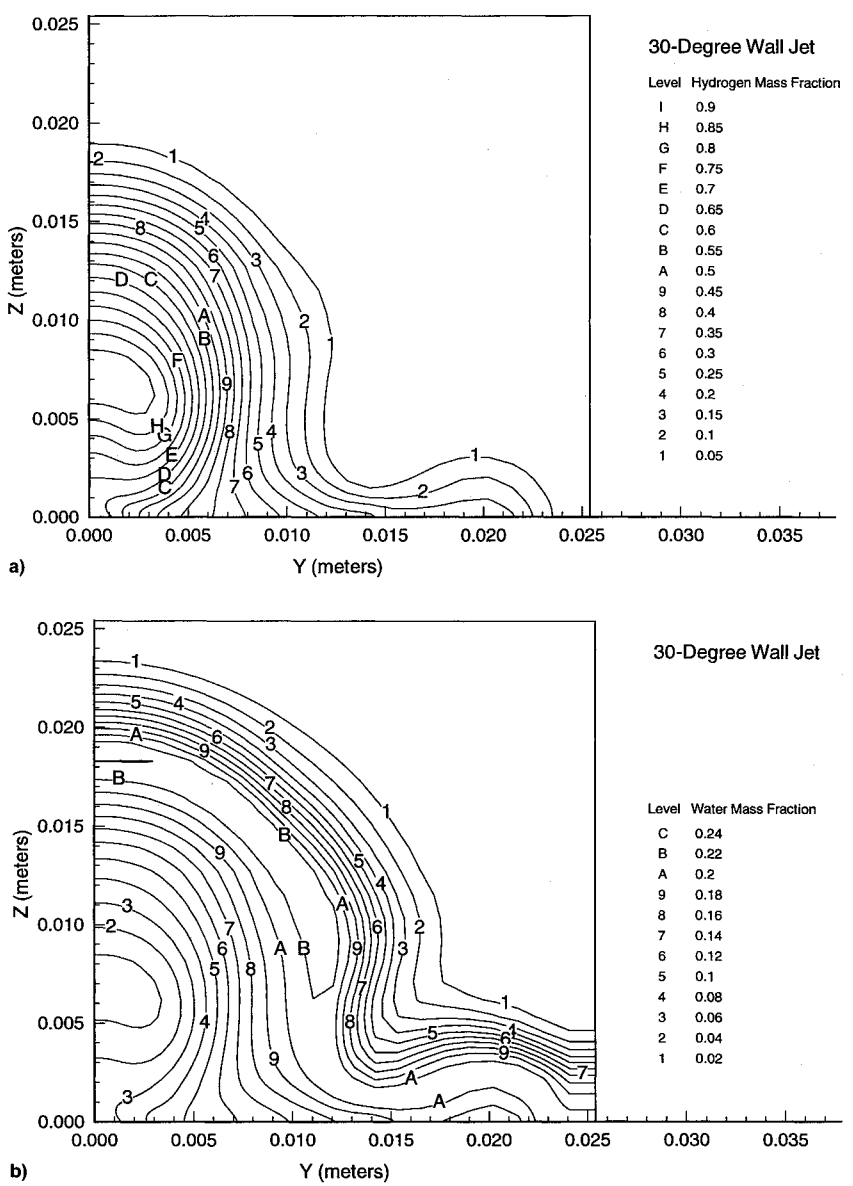

Fig. 3 Mass fraction contours on cross-sectional plane 4 cm downstream of jet for flush-wall injection (30-deg, flight Mach 17 enthalpy, fuel equivalence ratio = 3.0: a) hydrogen (H_2) and b) water (H_2O).

merically modeled with appropriate inflow and jet conditions. The second part of this section presents and discusses thrust potential axial and spatial distributions for these two cases.

Thirty-Deg Wall Jet Case (Mach 17 Enthalpy)

Figures 3a and 3b show downstream hydrogen and water mass fraction contours, respectively, for the 30-deg wall jet case. Contours shown are on a cross-sectional plane located at about 4 cm downstream of the injector. Due to the large injection angle of the 30-deg case and to the high fuel equivalence ratio of 3.0, spreading and penetration are significant. Considerable entrainment in the boundary layer is observed. Far downstream, this entrainment for the 30-deg case generates a distinct well-fueled region near the duct sidewall (modeled in this particular case as inviscid). Maximum water production occurs at or near the interface of the hydrogen jet core and the outer flow. This burning layer is large due to the fuel equivalence ratio of 3.0; water production has spread across much of the duct in the near field.

The mixing efficiency vs axial distance for the wall jet is shown in Fig. 4. Mixing is defined at each cross-sectional plane as the ratio of the integrated mass flux of the least available reactant if complete reaction takes place (with no further mixing) to the integrated total mass flux of the least available reactant. This parameter describes the degree of mixing of the fuel and the oxidizer and varies between 0 and 1. Mixing for the 30-deg wall jet case (with fuel equivalence ratio = 3.0) is rapid in the nearfield due to the large mass and momentum of the jet. This case reaches about a 90% mixed condition by the end of the duct.

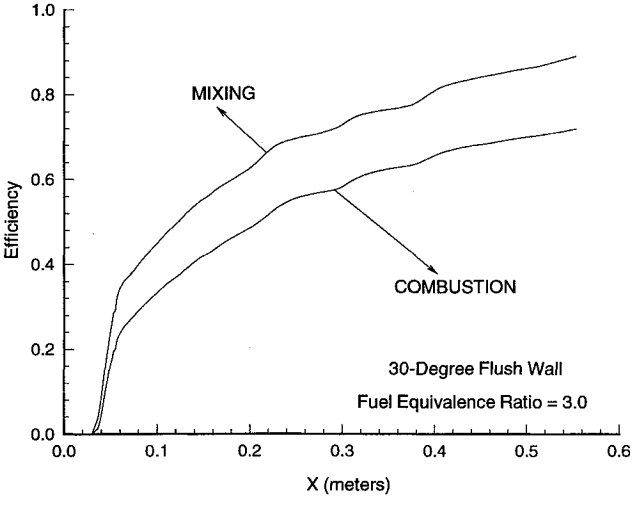

Fig. 4 Mixing and combustion efficiencies for 30-deg flush-wall injector (x axis origin located approximately 4 cm upstream of injector).

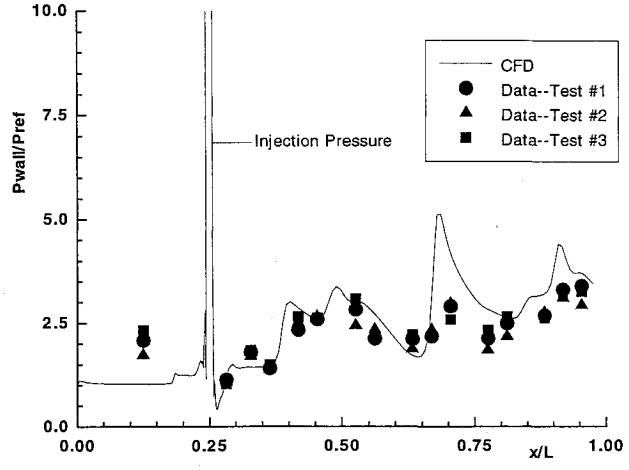

Fig. 5 Wall pressure axial distribution for 30-deg flush-wall injector (x axis includes entire duct).

Figure 4 also illustrates combustion efficiency vs axial distance for this case. Combustion efficiency is defined at each cross-sectional plane as the ratio of the integrated mass flow of least available reactant in water product to the total mass flow of least available reactant. Its upper limit is the mixing efficiency. Due to dissociation products such as H, O, and OH, the combustion efficiency is about 10–15% less than the mixing efficiency. Note that if the combustion efficiency is based on actual heat release in such flows, its magnitude would be even less than that shown here. Dissociation reactions are dominant in the Mach 17 flow presented here (due to the high inflow temperature).

Figure 5 is a plot of predicted wall pressure vs experimental wall pressure for the 30-deg (reacting) wall jet case. Agreement is reasonable in the near field of the injector. The predicted pressure distribution for the far field indicates a stronger reflecting shock structure than evident in the experimental data. This is at least partially due to the inviscid side wall modeled in the simulation.

Swept Ramp Injector (Mach 13.5 Flight Conditions)

In order to study the effects of higher pressure inflow, high fuel temperature, and intrusive injectors on combustor performance, a swept ramp calculation with reaction was performed using a high-pressure inflow (1.35 atm as opposed to 0.2 atm for the previous case) and high fuel static temperature (700 K). Fuel equivalence ratio was held at 1.0 for this case. Additionally, both a lower static temperature was used on the inflow (resulting in less dissociation in the flow) and higher wall temperatures in the duct were maintained. These conditions result in a subscale numerical prediction of swept ramp performance at (approximately) anticipated combustor entrance and injection conditions for Mach 13.5 flight.

Figure 6a illustrates hydrogen contours for this case at a cross-sectional plane located one ramp length downstream of the ramp base. There is slight warping of the fuel core due to the action of the large crossflow vortices generated by the ramp. Figure 6b is a plot of water mass fraction contours at the same plane. The characteristic lift of the swept-ramp jet has raised the reaction zone into the middle of the domain. Mixing and combustion efficiency vs axial distance are shown in Fig. 7. The combustion efficiency is about 20% less than the mixing efficiency at the end of the duct.

Thrust Potential

The remainder of this section discusses the results obtained by applying the thrust potential evaluation methods described earlier in this article. Figure 8a is a plot of combustor (net) specific thrust potential (i.e., net thrust potential per unit mass flow rate of air) vs axial distance in the duct for the flush-wall 30-deg injection case. The center of the injection orifice for the wall jet case shown in this section occurs at approximately 15 cm from the duct inflow, or, as shown in Fig. 8a, at 4 cm from the leading edge of the near-field solution (x = 0). The early and slight rise in thrust potential in Fig. 8a is believed to be due to a small amount of fuel entrainment upstream through the wall boundary layer. The large steep rise in thrust potential centered at about x = 5 cm is due to the downstream momentum addition of the jet; this rise is not vertical since the jet injection is spread axially along the bottom wall. This injector momentum is very large due to the high fuel equivalence ratio. There is a discernible rise in thrust potential in the near field due to reaction. Thrust potential is roughly constant across the first part of the combustor, although it begins to decrease in the midrange of the duct. Mixing and combustion efficiencies are high; the relatively flat thrust potential indicates that shock and friction losses (shear and convective heat transfer) and combustion heat-release are about evenly balanced in terms of thrust potential

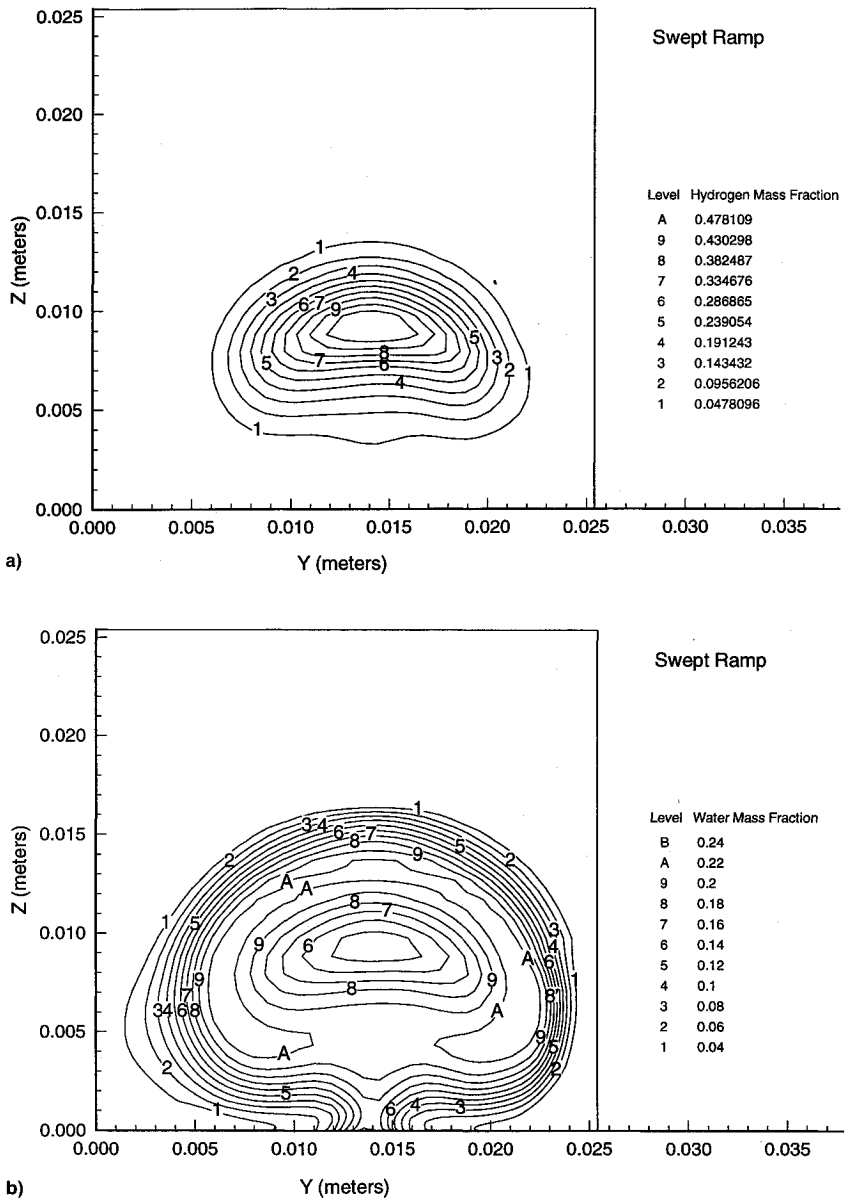

Fig. 6 Mass fraction contours on cross-sectional plane located one ramp length downstream of ramp base (flight Mach 13.5 enthalpy, fuel equivalence ratio = 1.0): a) hydrogen (H_2) and b) water (H_2O).

into the midrange of the combustor. In the latter half of the combustor, the losses begin to dominate the flow and the thrust potential begins to drop. The decrease in thrust potential with axial distance in this region is partially mitigated due to the modeling of the sidewall as inviscid (hence, less shear in the flow).

In order to simulate vehicle flight conditions, a swept ramp is modeled in the same duct with a high pressure inflow and a high fuel temperature (700 K). The flight Mach number is lowered for this case to 13.5 with an injected fuel equivalence ratio of 1.0. The thrust potential for this case is shown in Fig. 8b. The ramp leading edge is at $x = 0$ in Fig. 8b whereas the ramp itself is 4 cm long. The potential drops along the ramp as expected due to friction, pressure drag, and shocks. The vertical rise in thrust potential at $x = 4$ cm is due to the streamwise momentum contribution of the jet. The mixing and the reaction of the fuel then contributes to a gain in net thrust potential until $x = 20$ cm, at which station the peak potential is reached. The thrust then begins to decrease due to the local effect of the increasing losses. At the end of the duct, the thrust potential has been reduced to the level of the inflow potential. The major component of thrust potential gain is due to jet momentum in both wall jet and ramp cases. However, a large reaction-induced gain is clearly observed for the swept ramp at Mach 13.5 flight enthalpy.

Thrust Potential Spatial Distribution

Figure 9 shows contours of thrust potential on three cross-sectional planes for the 30-deg wall jet case. These planes are located at $x = 10$, 15, and 25 cm downstream of the injector, respectively. The flow near the top and bottom (note the side wall is inviscid) exhibit layers of negative thrust potential. These loss regions are associated with the shear in the boundary layers. There is a related zone of negative thrust potential where the jet core is located. This jet–core zone of loss has been observed in contours of total pressure for low-enthalpy mixing flows in both experimental and numerical studies.[16] The low thrust potential in this region is due to the lower velocities and temperatures in the unmixed fuel core. The region of high thrust potential due to reaction forms a shell around the structure of the jet with maximum thrust corresponding very roughly to stoichiometric conditions. The level of thrust potential is high and the region is relatively large. This zone of high potential moves toward the center of the

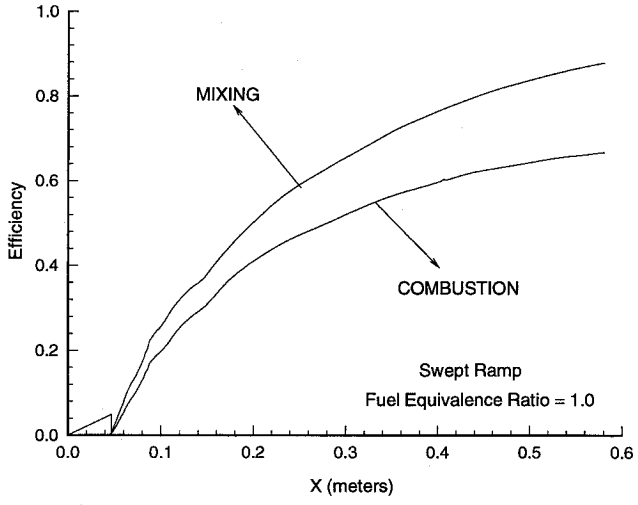

Fig. 7 Mixing and combustion efficiencies for swept ramp (x axis origin located at the ramp leading edge).

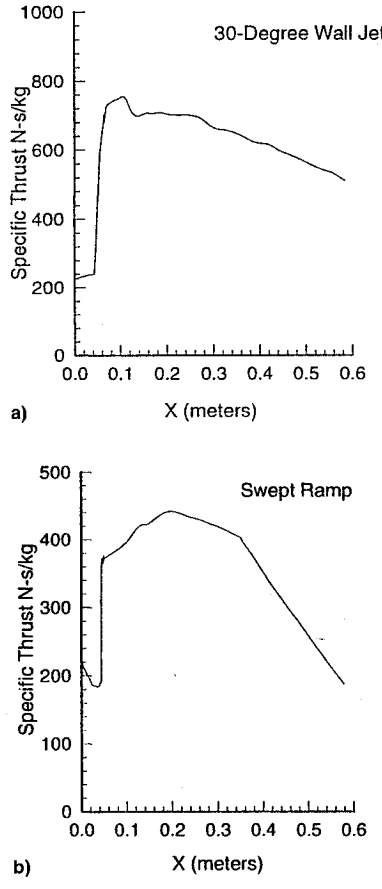

Fig. 8 Combustor thrust potential axial distribution: a) 30-deg flush-wall jet (fuel equivalence ratio = 3.0, flight Mach 17 enthalpy); x axis origin located approximately 4 cm upstream of injection and b) swept ramp (fuel equivalence ratio = 1.0, flight Mach enthalpy); x axis origin located at ramp leading edge).

domain as shown in the second plane. A small zone of negative thrust potential forms at the upper right-hand corner. By the last plane shown, the region of high thrust potential has approximately stabilized in the center of the domain and the upper right corner is dominated by the growth of the zone of negative thrust potential. However, there is little overall increase in the total negative thrust potential cross-sectional area across the axial length represented by these plots. This behavior corresponds with the observed flat curve of thrust potential shown in Fig. 8a for this case. The latter stage of the combustor (in which the thrust drops off significantly) is not shown in this sequence of planes.

Figure 10 is a similar sequence of thrust contours on cross-sectional planes downstream of the injection ramp for Mach 13.5 inflow conditions. These planes correspond to one, two, and three ramp lengths downstream of the base plane of the swept ramp, respectively. Since the hydrogen jet is injected from the sheltered base of the ramp, the core is coherent and, because of the hot fuel, forms a distinct region of high thrust potential in the first plane shown. Slight vortex-induced warping of the higher thrust potential zone is seen. However, the most apparent effect of the vortices and the ramp base on thrust potential is the entrainment of low potential flow up into the center of the domain from the lower wall loss region. In the second plane, the wall loss zones have visibly grown. However, the dominant feature as the flow evolves downstream is the increasingly important high thrust potential associated with the jet–air interface. This "shell" of high potential replaces the jet momentum core as the major feature by the second plane. The evolution of the wall loss zones (negative thrust potential) is inhibited by the strong reaction-induced potential gain in the last plane shown. Other possible features in this flow that could cause the suppression of the wall loss region include reaction in the boundary layer, turbulent mixing energization of the flow near the wall, or flow compression of the boundary layer itself. Note that the cross-sectional area covered by negative thrust potential is not appreciably different between the last two planes shown. In the last plane, the contours of high thrust potential clearly form a wide ring-like structure in the flow. The swept ramp case presented here exhibits the clear evolution of thrust potential in a realistic configuration.

Summary

A simple method for estimating the axial distribution of supersonic combustor thrust potential is presented. This method is based on one dimensionalizing a three-dimensional numerical solution in order to expand the flow to some defined reference conditions. Optimum combustor length can also be estimated using this method. As a complementary technique, the thrust potential of the flow in each individual cell in a CFD-generated flow plane can be calculated by a similar method. This leads directly to the ability to describe the spatial evolution and distribution of thrust potential, or conversely, flow losses. Mechanisms of thrust potential gain and loss can be studied using this approach. As the first part of this investigation, a wall jet case at a flow enthalpy corresponding to a flight Mach number of 17 has been presented. Although mixing is high for this flush-wall 30-deg injector at a very high fuel equivalence ratio, limited pressurization of the flow indicates general poor performance for this configuration for the flow conditions modeled. Note that the conditions used in this simulation were chosen in order to compare the CFD results with available experimental data from a pulse facility. A numerical case is then defined in which a swept ramp injector in the same confined duct is modeled with inflow and jet conditions more closely matched to actual combustor conditions at a flight Mach of 13.5. This results in a higher static pressure and a lower static temperature on the duct inflow (as well as higher fuel temperatures).

The methods developed for analyzing thrust potential are then applied to these cases. The axial distribution of overall combustor thrust potential displayed expected trends; the jet momentum is largely responsible for the gain in thrust potential. The 30-deg wall jet (with a high fuel equivalence ratio) exhibits a distinct effect of the reaction on thrust potential; for much of the duct the thrust potential does not decrease markedly. This indicates that the reaction is countering the losses. The reaction-induced thrust potential for the subscale

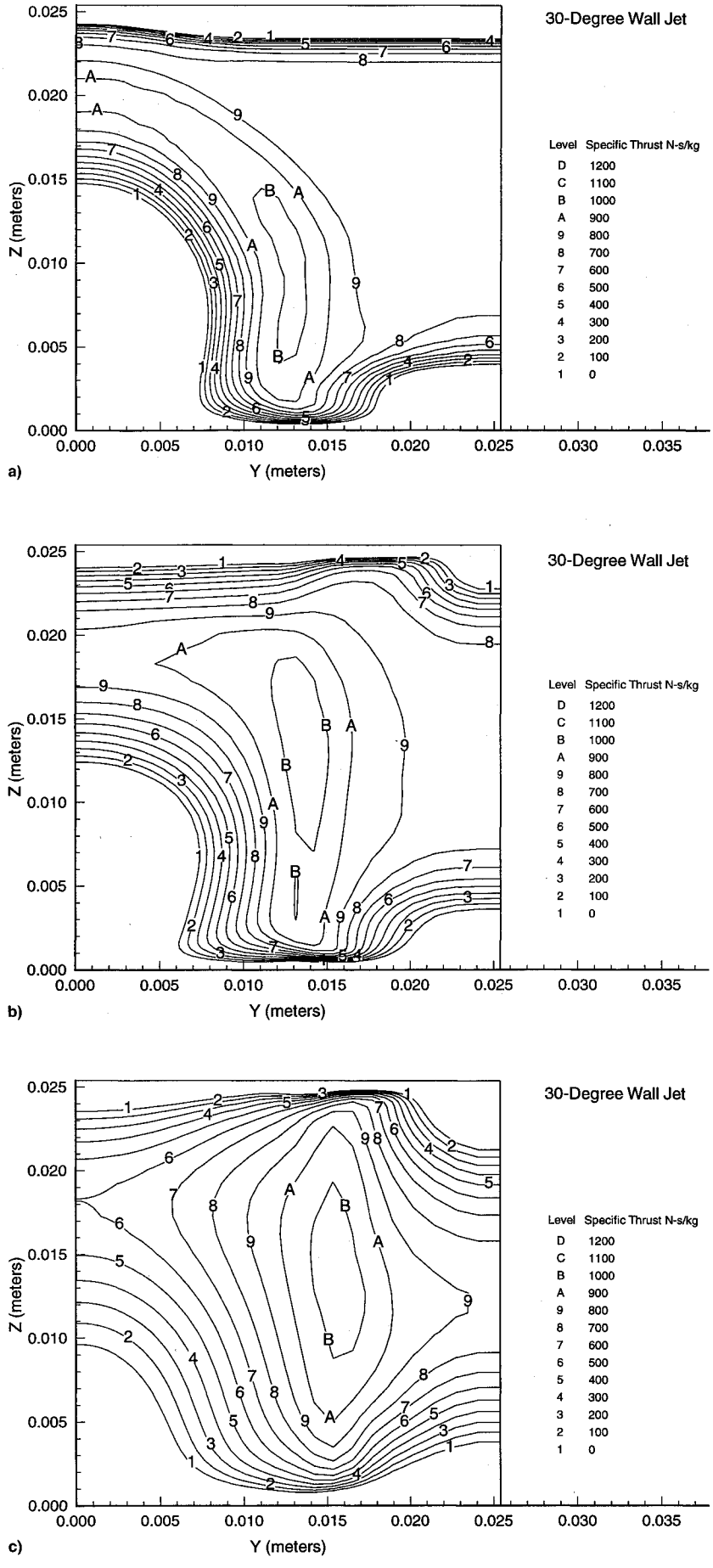

Fig. 9 Contours of thrust potential on cross-sectional planes for 30-deg flush-wall injection (fuel equivalence ratio = 3.0, flight Mach 17 enthalpy): a) 10, b) 15, and c) 25 cm downstream of injection.

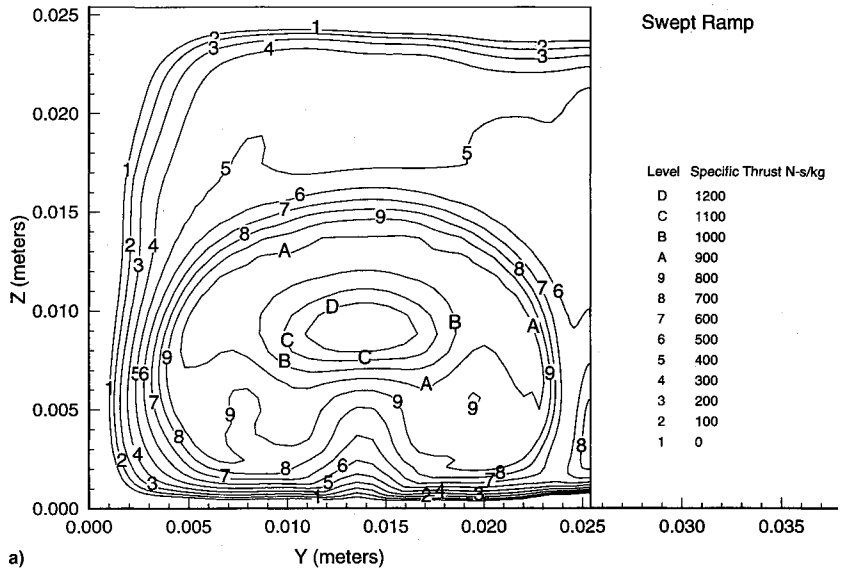

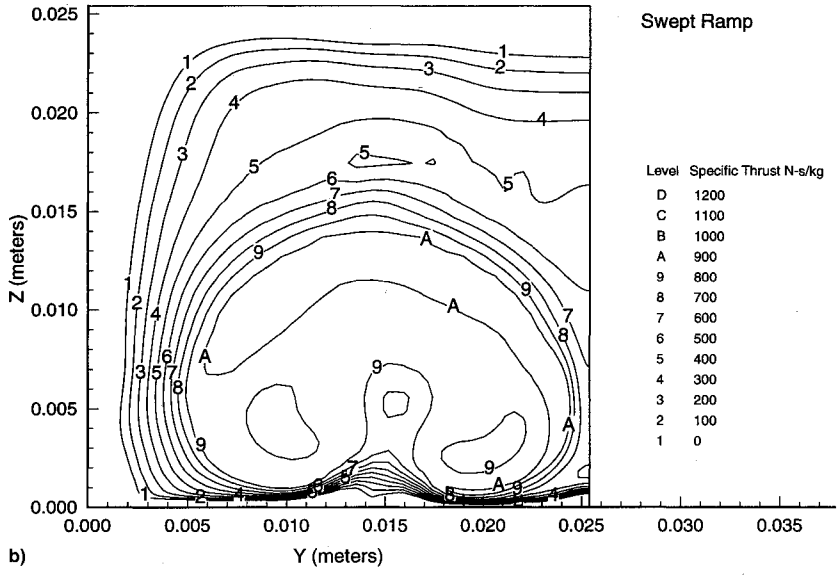

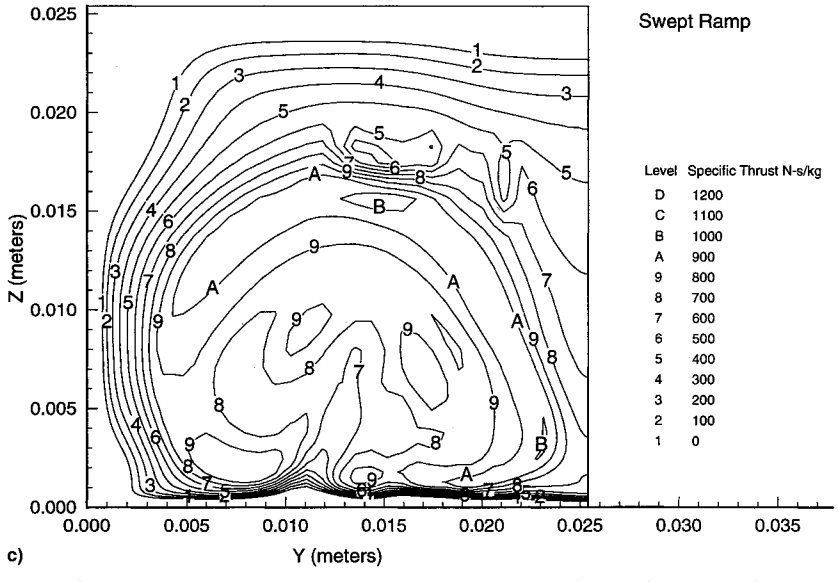

Fig. 10 Contours of thrust potential on cross-sectional planes for swept ramp injection (fuel equivalence ratio = 1.0, flight Mach 13.5 enthalpy): a) 1, b) 2, and c) 3 ramp lengths downstream of ramp base.

Mach 13.5 swept ramp case is more prominent due primarily to a lower flight Mach number, higher inflow pressures, and a high fuel temperature. A distinct peak in thrust potential downstream of the injector is observed for this case.

Finally, the study of the spatial distribution of thrust potential clearly supports the one-dimensionalized thrust potential axial distribution. The 30-deg wall jet case shows an approximate balance in thrust potential between the friction and the reaction across much of the combustor. Performance is enhanced by the reaction insomuch as a decrease in thrust potential is delayed until far downstream. A more interesting (and optimistic) spatial distribution of thrust potential is that obtained for the swept ramp ($M = 13.5$). In this case, the thrust potential clearly gains due to reaction across much of the combustor; the wall-bounded viscous loss regions have little or no net gain. The region of high thrust potential transitions from the jet momentum contribution in the near field to a ring-shaped zone of reaction-induced potential in the downstream flow.

References

[1]Riggins, D. W., Mekkes, G. L., McClinton, C. R., and Drummond, J. P., "A Numerical Study of Mixing Enhancement in a Supersonic Combustor," AIAA Paper 90-0203, Jan. 1990.

[2]Drummond, J. P., Carpenter, M. H., and Riggins, D. W., "Mixing and Mixing Enhancement in Supersonic Reacting Flowfields," *High-Speed Flight Propulsion Systems*, edited by S. N. B. Murthy and E. T. Curran, Vol. 137, Progress in Astronautics and Aeronautics, AIAA, Washington, DC, 1991, pp. 383–455.

[3]Bobskill, G., Bittner, R., Riggins, D. W., and McClinton, C. R., "CFD Evaluation of Mach 17 HYPULSE Scramjet Combustor Data," AIAA Paper 91-5093, Dec. 1991.

[4]Swithenbank, J., Eames, I., Chin, S., Ewan, B., Yang, Z., Cao, J., and Zhao, X., "Turbulence Mixing in Supersonic Combustion Systems," AIAA Paper 89-0260, Jan. 1989.

[5]Czysz, P., and Murthy, S. N. B., "Energy Analysis of High-Speed Flight Systems," *High-Speed Flight Propulsion Systems*, edited by S. N. B. Murthy and E. T. Curran, Vol. 137, Progress in Astronautics and Aeronautics, AIAA, Washington, DC, 1991, pp. 143–235.

[6]Builder, C. H., "On the Thermodynamic Spectrum of Air-Breathing Propulsion," AIAA Paper 64-243, June 1964.

[7]Riggins, D. W., and McClinton, C. R., "A Computational Investigation of Flow Losses in a Supersonic Combustor," AIAA Paper 90-2093, July 1990.

[8]Riggins, D. W., and McClinton, C. R., "Analysis of Losses in Supersonic Mixing and Reacting Flows," AIAA Paper 91-2266, July 1991.

[9]Bakos, R. J., Tamango, J., Rizkalla, O., Pulsonetti, M. V., Chinitz, W., and Erdos, J. I., "Hypersonic Mixing and Combustion Studies in the GASL HYPULSE Facility," AIAA Paper 90-2095, July 1990.

[10]Drummond, J. P., Rogers, R. C., and Hussaini, M. Y., "A Detailed Numerical Model of a Supersonic Reacting Mixing Layer," AIAA Paper 86-1427, June 1986.

[11]Carpenter, M. H., "Three-Dimensional Computations of Cross-Flow Injection and Combustion in a Supersonic Flow," AIAA Paper 89-1870, June 1989.

[12]Kamath, H., "Parabolized Navier-Stokes Algorithm for Chemically Reacting Flows," AIAA Paper 89-0386, Jan. 1989.

[13]McClinton, C. R., "CFD Support of NASP Design," AIAA Paper 90-3252, Sept. 1990.

[14]Mao, M., Riggins, D. W., and McClinton, C. R., "Numerical Simulation of Transverse Fuel Injection," *CFD Symposium on Aeropropulsion*, NASA CP 10045, Paper 37, April 1990.

[15]Eklund, D. R., Fletcher, D. G., Hartfield, R. J., McDaniel, J. C., Northern, G. B., Dancey, C. L., and Wang, J. A., "Computational/Experimental Investigation of Staged Injection into a Mach 2 Flow," *AIAA Journal*, Vol. 32, No. 5, 1994, pp. 907–916.

[16]Riggins, D. W., and McClinton, C. R., "A Computational Investigation of Mixing and Reacting Flows in Supersonic Combustors," AIAA Paper 92-0626, Jan. 1992.

[17]Reynolds, A. J., "The Variation of Turbulent Schmidt Numbers in Wakes and Jets," *International Journal of Heat and Mass Transfer*, Vol. 19, No. 7, 1976, pp. 757–764.